Acoustic Analogy with High-order Time Derivatives for Far-Field Acoustic Predictions

Minjun Park[*] and Hakjin Lee[†]

[*] *Avionics R&D center, Hanwha systems, Bundang, Gyeonggi-do, 13591, South Korea*

[†]*School of Mechanical and Aerospace Engineering, Gyeongsang National University, Jinju, Gyeongnam, 52828, South Korea*

Abstract

This paper proposes a numerical method for predicting the far-field noise using Ffowcs Williams-Hawkings (FW−H) equation with high-order finite-difference method for the time derivative. The results of this method for second-, fourth-, and sixth-order finite difference approximations are compared with that of analytic applications, such as monopole and dipole. It is observed that the use of the high-order time derivatives is an efficient approach to improve the prediction accuracy of the radiated acoustic pressure, particularly when the temporal resolution is not sufficiently high owing to the limited time step size. Our findings in this study provide evidence that for higher-order approximations, the RMS error for the first and second derivatives is smaller. In addition, the RMS error for the sixth-order approximation decreases considerably compared to that for the second-order approximation, with an increase in the number of points per period. This study and its results are expected to serve as a guide for noise prediction, indicating the temporal accuracies of the acoustic analogy according to the high-order approximation of time derivatives.

Keywords: Aeroacoustics, Acoustic analogy, Ffowcs Williams and Hawkings equation, High-order time derivative, Temporal accuracy

[†]Corresponding author's email: hlee@gnu.ac.kr

1. Introduction

With the improvements in the computational capacity of computers and the advent of powerful clusters, computational fluid dynamics (CFD) has emerged as a useful tool to solve engineering problems involving aerodynamic noise predictions [1, 2]. The results of CFD simulations can provide an insight into the noise generation mechanism and complex flow physics in the near field of sound sources, especially when the experimental methods are extremely demanding. However, the simulation process still requires a substantial amount of computational resources, thus resulting in increased costs associated with the high-density grids and small size of time steps to calculate far-field acoustics. In addition, the grid-based CFD method experiences excessive numerical dissipation on coarse grids; hence, the acoustic wave tends to dissipate quickly after traveling from the noise source. Therefore, high-order and high-resolution numerical schemes have been proposed to compute far-field acoustic pressures and acoustic fields near sources.

The most commonly employed technique for predicting far-field noise is the acoustic analogy approach, which utilizes the Ffowcs Williams-Hawkings (FW-H) equation [3]. This is primarily because the direct application of CFD simulations to obtain the acoustic solution is a time-consuming process. Hence, the prediction of acoustic sources using CFD simulations and that of acoustic wave propagation using the integral formulation of acoustic analogy are combined to calculate the resulting far-field noise [4-6]. Although this hybrid method is efficient and useful approach to evaluating the far-field acoustic, its applications can be limited by the quality of input data, such as spatial and temporal resolutions, obtained from either the numerical simulations or measured pressure data from wind tunnel tests [7, 8]. Typically, the time step size used in numerical simulations is much smaller than the time step needed to accurately capture the acoustic waves in the calculations. This is because the temporal resolution of the simulations is determined by the smallest step in the spatial grid [9]. Hence, previous studies [10-13] focused on improving spatial resolution with high-order and high-resolution numerical scheme for capturing the details of acoustic features near the sources more accurately.

The literature survey showed that the temporal resolution plays a critical role in ensuring the precision of noise calculations. Ziegenbein and Oh [14] revealed that sufficient temporal resolution is required to achieve good agreement between experimental results and predictions when blade vortex interaction (BVI) occurs. The time-resolved particle image velocimetry (PIV) measurement

has been used to obtain the input data to predict far-field noise [15-17]. It was reported that insufficient temporal resolution leads to spurious high intensity source terms [16] and a significant Taylor truncation error [17]. Brentner et al. [18] investigated the temporal resolution effects on the noise prediction accuracy of BVI events using the experimental data from the DNW model [19]. They compared the acoustic predictions calculated by the measured data with the different rates of 256, 512, and 1024 points per rotor revolution (pts/rev). It is found that 1024 pts/rev is sufficient to predict the peak amplitude of BVI noise using straightforward second-order accurate, central difference approximation in the temporal scheme.

Although the temporal order of the time derivative for acoustic analogy is the important factor, as well as temporal resolutions, limited research has been devoted toward improving the temporal accuracy of acoustic propagation. The FW–H acoustic analogy with a second-order finite-difference approximation for the time derivative is more generalized for far-field acoustic predictions [20-22]. Hence, it is essential to develop a higher-order finite-difference method for the time derivative, in order to predict the radiated noise associated with high frequencies for a limited time step size in the numerical simulations. This is because a smaller step size significantly increases the required computational time and increasing the time step while maintaining accuracy can be used to reduce the amount of data stored.

This paper proposes a numerical technique for predicting aerodynamic noise to improve temporal accuracy using the FW–H equation with high-order time derivatives. The impacts of second-, fourth-, and sixth-order finite-difference approximations for the time derivatives were examined by solving analytic application problems, such as those involving monopole and dipole sources. The numerical results highlighted the advantages of using a higher-order scheme. Moreover, the findings of this study are expected to serve as a guide for improving the numerical accuracy of higher-order time derivatives for predicting acoustic propagation in order to determine the target frequency.

2. Numerical method

2.1. Ffowcs Williams and Hawkings (FW–H) equation

Lighthill [23, 24] first suggested the concept of acoustic analogy with a formulation based on the mass and momentum conservation equations of the compressible Navier–Stokes equation. This

formulation describes the theory of aerodynamic sound generation and radiation as a result of fluctuating fluid flow, as distinct from the sound produced by the vibration of solids. Curle [25] modified Lighthill's acoustic analogy for considering the effect of solid boundaries. Ffowcs Williams and Hawkings [3] derived the FW–H equation to account for the effect of solid boundaries in arbitrary motion using generalized functions. Further, Lowson [26, 27] and Farassat [28, 29] applied the FW–H equation to predict rotor noise. Di Francescantonio [30] used the FW–H equation with a permeable surface as the Kirchhoff approach [31, 32] to capture the quadrupole noise associated with the high-speed impulsive noise of helicopter rotors. Farassat formulated the integral solution of the FW–H equation, which is one of the most important formulae in the field of aeroacoustics and is usually employed for hybrid computation [33-35].

In this study, we employed the acoustic analogy approach, utilizing time-domain integral formulations of the FW-H equation with a permeable surface, to predict far-field noise. The FW-H equation, derived from the rearrangement of the Navier-Stokes equations, takes the form of an inhomogeneous wave equation. It includes a volume source term (quadrupole) and two surface source terms (dipole and monopole) [36]; this is expressed in Eq. (1). The first term on the right-hand side (RHS) of Eq. (1) indicates the flow-induced noise, and the second and third terms denote the loading and thickness noises, respectively. This equation provides an accurate theoretical solution for describing the noise propagation from the acoustic source to the observer at the far field.

$$\Box^2 p'(\mathbf{x},t) = \frac{\partial^2}{\partial x_i \partial x_j}[T_{ij}H(f)] - \frac{\partial}{\partial x_i}[L_i\delta(f)] + \frac{\partial}{\partial t}[\rho_o U_n]\delta(f) \tag{1}$$

where **x** is an observer position, t is the observer time, and p' is the acoustic pressure at the observer position. The term with the subscript of o indicates the fluid variables at the quiescent medium in the RHS of Eq. (1). $H(f)$ is the Heaviside function, and $\delta(f)$ is the Dirac delta function.

The Lighthill stress tensor T_{ij} represents the volume source term with quadrupole acoustic radiation [24].

$$T_{ij} = \rho v_i v_j + p_{ij} - c_o^2(\rho - \rho_o)\delta_{ij} \tag{2}$$

L_i is the unsteady loading vector on the source surface, which is the dipole source term, and U_n is the unsteady flow vector of the source, which is the monopole source term, as in Eqs. (3) and (4).

$$L_i = \Delta p_{ij} n_j + \rho u_i (u_n - v_n) \tag{3}$$

$$U_n = \rho_o v_n + \rho (u_n - v_n) \tag{4}$$

where u_n and v_n are the fluid and perturbation velocities normal to the source surface, respectively.

On comparing Eq. (1) with Lighthill's formulation, it can be observed that the source term in the FW–H equation contains two more components for representing monopole and dipole sources, in addition to the Lighthill's stress tensor. The volume source term in the FW–H equation can be omitted to avoid complicating the volume integration in practical applications. Farassat derived the integral solution of the FW–H equation, termed Farassat's formulation 1A, by neglecting the quadrupole source term. This formulation only contains the thickness and loading source terms, as shown in Eq. (5), because the quadrupole source term has already been included in the permeable surface [37]. The subscripts T and L correspond to the thickness and noise components, respectively.

The FW-H equation has been utilized for permeable surfaces encompassing all physical noise sources, thereby eliminating the necessity to calculate the quadrupole contribution:

$$p'(\mathbf{x},t) = p'_T(\mathbf{x},t) + p'_L(\mathbf{x},t) \tag{5}$$

$$p'_T(\mathbf{x},t) = \frac{1}{4\pi} \int_{f=0} \left[\frac{\rho_o (\dot{U}_n + U_{\dot{n}})}{r \left| 1 - M_r \right|^2} \right]_{ret} dS + \frac{1}{4\pi} \int_{f=0} \left[\frac{\rho_o U_n (r\dot{M}_r + cM_r - cM^2)}{r^2 \left| 1 - M_r \right|^3} \right]_{ret} dS \tag{6}$$

$$\begin{aligned} p'_L(\mathbf{x},t) = {} & \frac{1}{4\pi c} \int_{f=0} \left[\frac{\dot{L}_r}{r \left| 1 - M_r \right|^2} \right]_{ret} dS + \frac{1}{4\pi} \int_{f=0} \left[\frac{L_r - L_i M_i}{r^2 \left| 1 - M_r \right|^2} \right]_{ret} dS \\ & + \frac{1}{4\pi c} \int_{f=0} \left[\frac{L_r (r\dot{M}_r + cM_r - cM^2)}{r^2 \left| 1 - M_r \right|^3} \right]_{ret} dS \end{aligned} \tag{7}$$

$$\tau = t - \frac{r}{c} \tag{8}$$

where $[\ ]_{ret}$ in Eqs. (6) and (7) indicates that the values enclosed within the symbol are assessed at the retarded-time (τ), defined as in Eq. (8). Here, r is the radiation distance from the source

position (**y**) to the observer position (**x**), and c is the speed of sound. The observer time (t) corresponds to the moment when the sound reaches the observer's location. On the other hand, the retarded time or source time (τ) refers to the time at which the acoustic signal that reaches the observer at time (t) was originally emitted from the source. The RHSs of Eqs. (6) and (7) are mainly associated with the local acceleration of the surface and the net force acting on the fluid, respectively. The dots imply the time derivative terms, i.e., $\dot{U}_n$, $\dot{L}_r$, and $\dot{M}_r$. Therefore, the order of the finite-difference approximation for the time derivative can affect the accuracy of the numerical predictions.

2.2. Source-time dominant algorithm

The numerical algorithm is required to provide the acoustic solution from the analytical formulation. The most common methods for finding the time history of the acoustic pressure are the retarded-time algorithm or source-time dominant algorithm. For the retarded-time algorithm, it is necessary to maintain a fixed observer position ($\boldsymbol{x}$) and observer time (t) throughout the numerical integration process. Although the retarded-time approach has proven to be robust, the coordinate transformation for each point on the noise source grid is needed to find the particular source time, hence satisfying the retarded-time equation in Eq. (8) for each observer time at which the solution is desired. The source-time dominant algorithm presents an alternative to the retarded-time approach. In this method, the source time (τ) is fixed in advance instead of determining the observer time and estimating when the acoustic signal will reach the observer. This method offers a different perspective by focusing on the emission time from the source rather than the arrival time at the observer. Although the traveling time from each source point to the observer location is different, the observer time can be computed analytically by adding the traveling time to the emitted source time; hence, determining the observer time is more straightforward than finding the retarded time. In the source-time dominant approach, a sequence of observer times is generated, which are unequally spaced. To combine the contributions from all noise sources at a specific observer time, it is essential to interpolate the time history of the acoustic signal at the observer position. This interpolation process ensures that the acoustic signals from different noise sources are synchronized and can be summed together. The source-time dominant algorithm is more useful for predicting the far-field noise using the discrete time-dependent input data obtained from CFD

simulation [20, 38, 39]. In addition, since the calculation process of this algorithm is inherently parallel, efficient memory management is possible for massive computation [40].

In this study, the source-time dominant algorithm is implemented for predicting the radiated acoustic pressure at the observer position, and its schematic diagram is shown in Fig. 1. First, choose a source panel with a whole source time signal based on the center of the panel, and then calculate when the signal reaches the observer. After finding the observer time emitted from the source panel, calculate the time derivative of the fluid properties from the source panel and compute radiated acoustic pressure at the observer position using Eqs. (6) and (7). Lastly, a single loop is completed when the acoustic signal for the observer position is interpolated to store at the desired observer time with the equal time step size. The Lagrange polynomial interpolation [41] is utilized in this study.

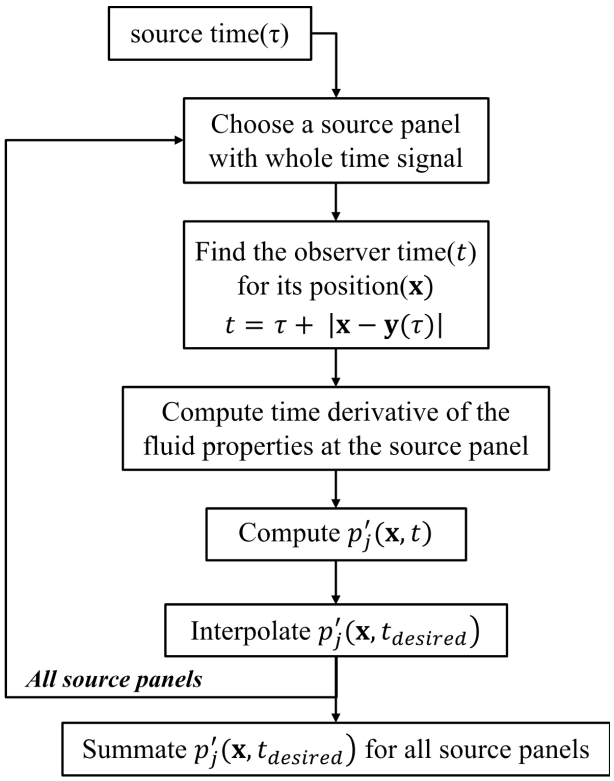

Fig. 1. Schematic of the source-time dominant algorithm.

The source-time dominant algorithm can be simplified to one forward calculation at each source time (τ) by assuming that the observers are stationary and the sources are moving. The forward calculation of time is essential not just for determining the source position, but also for evaluating the velocity and acceleration of the source panel. The source-time dominant algorithm appears to

be efficient. However, when high temporal resolution is necessary, such as in predicting blade-vortex interaction (BVI) noise [38] and other impulsive noise sources [20], the source-time history may require a greater number of data points compared to the acoustic-pressure time history. This requirement for additional data points can have an impact on the reduction of computational efficiency. The computational cost can be efficiently alleviated by applying high-order time derivatives into the source-time dominant algorithm.

2.3. Higher-order finite-difference method for the time derivative

The second-order central difference approximation for the time derivative is generally employed for the FW–H acoustic analogy in the time domain [20, 21]. In this study, the effect of the higher-order finite-difference method on the accuracy of predictions of the far-field noise is investigated. The second-, fourth-, and sixth-order central difference approximations for the first and second derivatives in time can be formulated as shown in Eqs. (9)–(11) and Eqs. (12)–(14), respectively, where the superscript j represents the index for the source time step.

$$v_i = \left.\frac{\partial \mathbf{y}}{\partial \tau}\right|^j = \frac{\mathbf{y}^{j+1} - \mathbf{y}^{j-1}}{2(\Delta\tau)} + O(\Delta\tau)^2 \tag{9}$$

$$v_i = \left.\frac{\partial \mathbf{y}}{\partial \tau}\right|^j = \frac{-\mathbf{y}^{j+2} - 8\mathbf{y}^{j-1} + 8\mathbf{y}^{j-1} - \mathbf{y}^{j-2}}{12(\Delta\tau)} + O(\Delta\tau)^4 \tag{10}$$

$$v_i = \left.\frac{\partial \mathbf{y}}{\partial \tau}\right|^j = \frac{\mathbf{y}^{j+3} - 9\mathbf{y}^{j+2} + 45\mathbf{y}^{j+1} - 45\mathbf{y}^{j-1} + 9\mathbf{y}^{j-2} - \mathbf{y}^{j-3}}{60(\Delta\tau)} + O(\Delta\tau)^6 \tag{11}$$

$$\dot{v}_i = \left.\frac{\partial^2 \mathbf{y}}{\partial \tau^2}\right|^j = \frac{\mathbf{y}^{j+1} - 2\mathbf{y}^{j} + \mathbf{y}^{j-1}}{(\Delta\tau)^2} + O(\Delta\tau)^2 \tag{12}$$

$$\dot{v}_i = \left.\frac{\partial^2 \mathbf{y}}{\partial \tau^2}\right|^j = \frac{-\mathbf{y}^{j+2} + 16\mathbf{y}^{j+1} - 30\mathbf{y}^{j} + 16\mathbf{y}^{j-1} - \mathbf{y}^{j-2}}{12(\Delta\tau)^2} + O(\Delta\tau)^4 \tag{13}$$

$$\dot{v}_i = \left.\frac{\partial^2 \mathbf{y}}{\partial \tau^2}\right|^j = \frac{2\mathbf{y}^{j+3} - 27\mathbf{y}^{j+2} + 270\mathbf{y}^{j+1} - 490\mathbf{y}^{j} + 270\mathbf{y}^{j-1} - 27\mathbf{y}^{j-2} + 2\mathbf{y}^{j-3}}{180(\Delta\tau)^2} + O(\Delta\tau)^6 \tag{14}$$

The accuracies of the second-, fourth-, and sixth-order central difference approximations were compared with the analytic solution before implementing the high-order time derivative in

Farassat's Formulation 1A. We assumed an analytic function with magnitude $A = 1$, frequency $f = 1$ Hz, and $\varphi = 0$, as defined in Eq. (15). Thus, the first- and second-order time derivatives of the analytic function can be expressed as in Eqs. (16) and (17), respectively:

$$y = A\sin(\omega\tau + \varphi) \tag{15}$$

$$v_{\text{analytic}} = \frac{\partial y}{\partial \tau} = A\omega\cos(\omega\tau + \varphi) \tag{16}$$

$$\dot{v}_{\text{analytic}} = \frac{\partial^2 y}{\partial \tau^2} = -A\omega^2\sin(\omega\tau + \varphi) \tag{17}$$

The comparison condition for calculating the time derivatives is 8 points per period. Fig. 2(a) shows that the second-order approximation of the first derivative tends to underpredict the peak values, whereas the fourth- and sixth-order approximations yield similar results. However, when predicting the second derivative, the sixth-order finite-difference approximation shows better agreement with the analytic solution, as compared with the second- and fourth-order formulae, as shown in Fig. 2(b). Based on our findings, it can be observed that the higher-order formulae of finite-difference approximations achieve better results for the predictions of first and second derivatives. Fig. 3 presents a comparison of the root mean square (RMS) error for the different orders of finite-difference approximations depending on the number of points per period. It is evident that, for higher-order approximations, the RMS error for the first and second derivatives is smaller. In addition, the RMS error for the sixth-order approximation decreases considerably compared to that for the second-order approximation, with an increase in the number of points per period. Thus, the sixth-order central finite-difference approximation of the first and second derivatives provided a more accurate solution than the results obtained by the second- and fourth-order approximations. The effects of the higher-order formulae of the finite-difference approximations on the prediction accuracy of acoustic radiation for monopole and dipole sources are discussed in the following section.

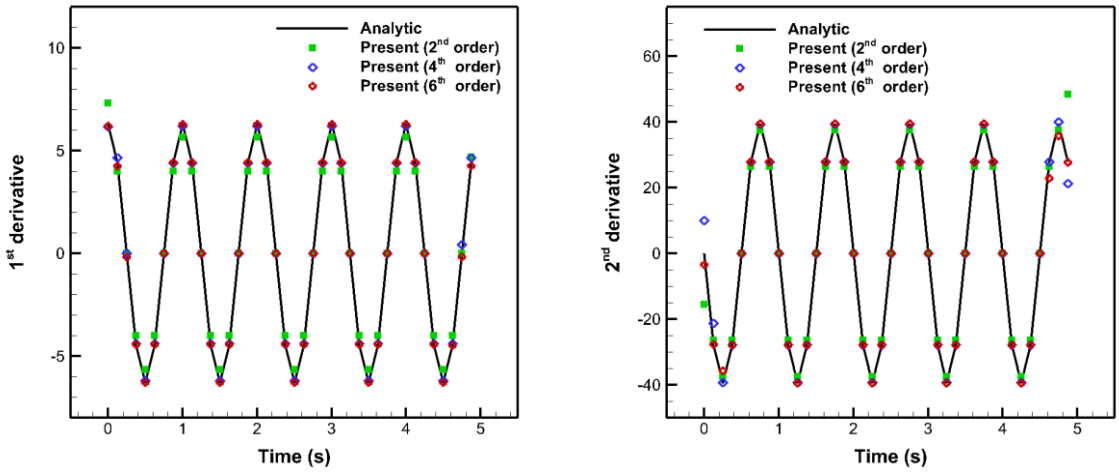

Fig. 2. Comparison of second-, fourth-, and sixth-order finite-difference approximations at 8 points per period: (a) first derivative and (b) second derivative.

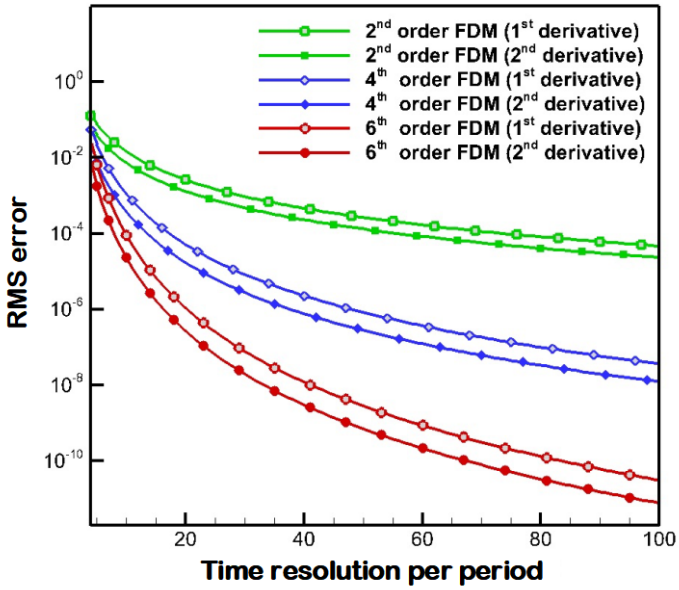

Fig. 3. Comparison of RMS error based on the number of points per period for second-, fourth-, and sixth-order finite-difference approximations of the first and second derivatives.

3. Validation and results

The acoustic analogy code based on the FW–H equation with the higher-order finite-difference method for the time derivative was applied to predict the acoustic pressure radiated from the sound sources that were analytically modeled using the stationary monopole and dipole point sources, as shown in Eqs. (18) and (19), respectively [42]. Both point sources satisfy that the source distributions are compact. The monopole source has an omnidirectional radiation pattern, whereas the dipole source has a directional characteristic along the x_2-axis. As shown in Fig. 4, both the point sources are located at the origin and covered by a Kirchhoff (permeable) surface [32]. The acoustic pressures on the Kirchhoff surface with a radius of 1 m were established based on the radiation of the monopole and dipole sources with a magnitude A = 1 and frequency f = 10 Hz. The observers were placed at a distance of 15 m from the acoustic source position. The data consist of velocity, pressure, and density obtained from the velocity potential function and linearized Euler equation, as in Eq. (20).

$$\phi(\mathbf{x},t)_{monopole} = \frac{A}{4\pi r}\exp\left[i\omega\left(t-\frac{r}{c}\right)\right]_{ret} \tag{18}$$

$$\phi(\mathbf{x},t)_{dipole} = \left\{-\frac{Ax_2}{4\pi r^3}\exp\left[i\omega\left(\tau-\frac{r}{c}\right)\right]_{ret} - \frac{iAkx_2}{4\pi r^2}\exp\left[i\omega\left(\tau-\frac{r}{c}\right)\right]_{ret}\right\} \tag{19}$$

$$\mathbf{u} = \nabla\phi, \quad p' = -\rho_0\frac{\partial\phi}{\partial t}, \quad \rho' = \frac{p'}{c^2} \tag{20}$$

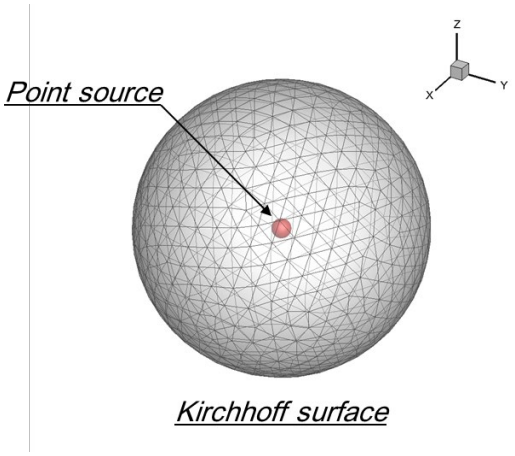

Fig. 4. Point source covered by Kirchhoff surface with radius 1m.

Figure 5 depicts the directivity of the acoustic pressure radiated from each acoustic source with a target frequency of f = 10 Hz. The validation results are obtained via the second-order approximation of the first- and second-time derivatives in high temporal resolutions, with 32 points per period for minimizing numerical errors. On comparing the results, it was observed that both the directivity and magnitude of the acoustic pressure are consistent with the analytic solution computed using Eqs. (18) and (19), respectively. Fig. 6 shows the comparison of the prediction of the acoustic pressure signal with the analytic solutions at a radiation directivity of 90º. It can be seen that the acoustic pressure signals of the monopole and dipole source are well-matched with the analytic solutions. However, the acoustic analogy with the low-order approximation of the time derivative provides accurate results for conditions where the resolutions per period are high. In low time resolutions per period, the prediction results of the lower-order approximation of time derivatives might have lower accuracies than those of the higher-order approximation. The prediction results for low time resolutions per period were compared with the acoustic pressure signals obtained by applying the N^{th}-order approximation of the time derivatives for 8 points per period. Fig. 7 shows that the results of the fourth- and sixth-order approximations are in close agreement with the analytic solution, whereas those of the second-order approximation tend to underpredict the acoustic pressure. It is observed that when the time resolutions per period are not sufficiently high, the acoustic analogy with the higher-order approximation provides more accurate predictions than that with the lower-order approximation.

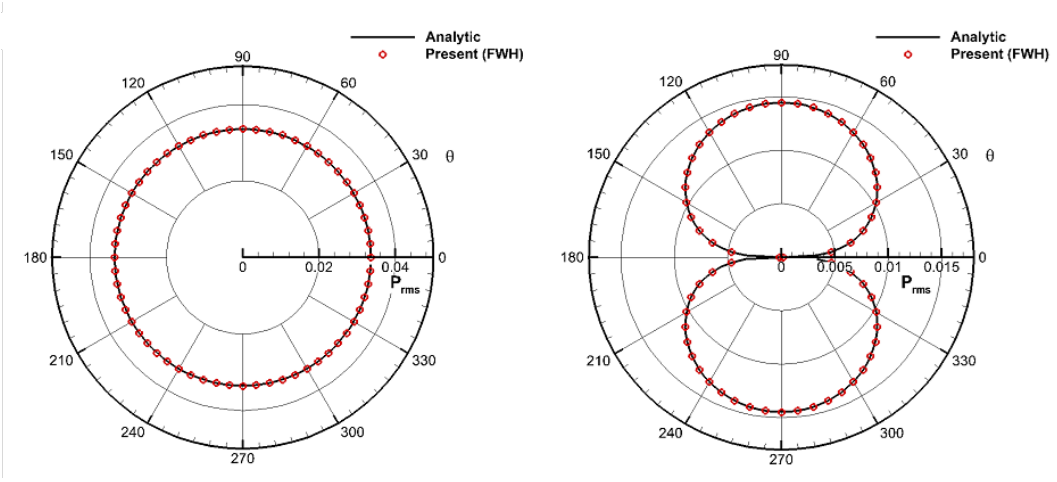

(a) (b)

Fig. 5. Validation of radiated acoustic directivity for magnitude $A = 1$, frequency $f = 10$ Hz: (a) monopole source and (b) dipole source.

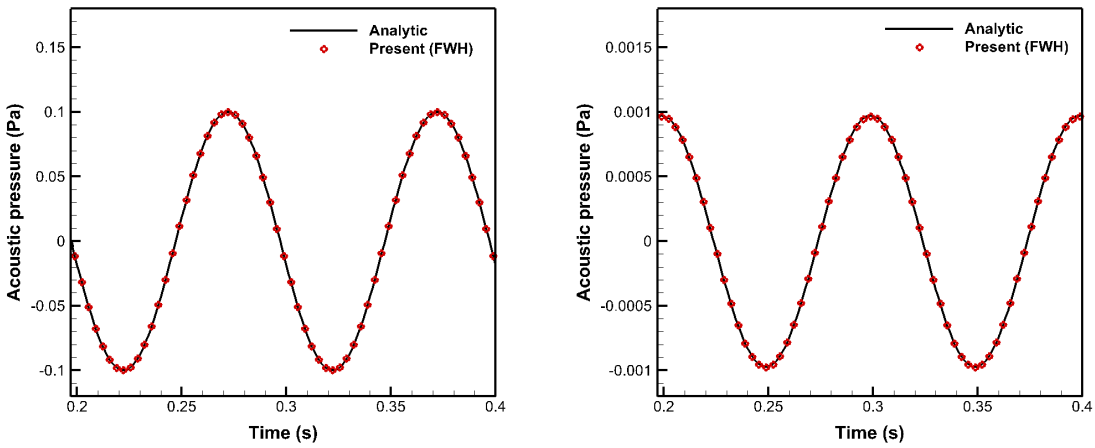

(a) (b)

Fig. 6. Comparison of the predicted acoustic pressure signals with second-order finite-difference approximations of time derivatives for 32 points per period and analytic solutions at a radiation directivity of 90º: (a) monopole source and (b) dipole source.

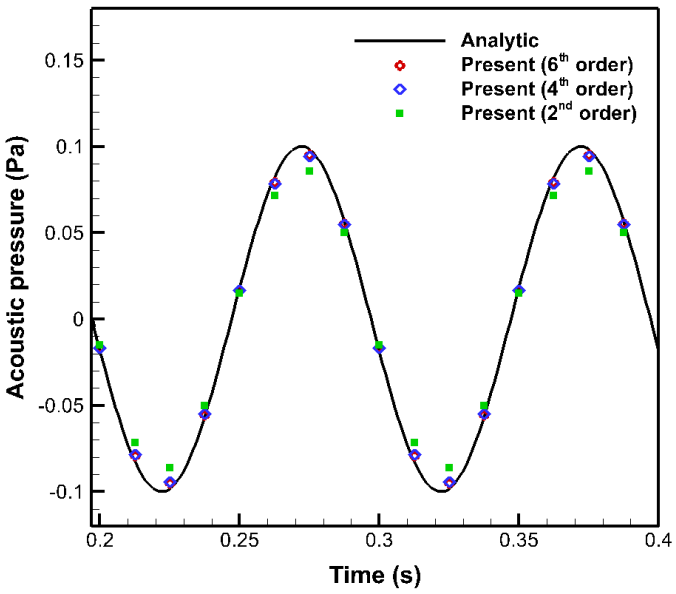

Fig. 7. Comparison of radiated acoustic pressure signals obtained from monopole source (magnitude $A = 1$, frequency $f = 10$ Hz) for 8 points per period with second-, fourth-, and sixth-order finite-difference approximations of time derivatives.

Figure 8 shows a comparison of the accuracy of the numerical results obtained from the acoustic analogy with the second-, fourth-, and sixth-order approximations of the time derivatives depending on the time resolutions per period. The accuracy of the acoustic prediction along the y-axis can be defined as the numerical prediction results divided by the exact solutions. That is, the closer it is to 1, the more accurately predicted it is. The x-axis denotes the time resolutions per period, indicating that the temporal resolution of the predictable target frequency can be altered based on the predetermined time step size. For higher temporal resolutions (exceeding 16 points per period), the analytic solutions differ from all numerical prediction results by less than 4%. However, in low temporal resolutions (less than 16 points per period), the numerical results of the fourth- and sixth-order approximations are approximately 2–16% more accurate than those of the second-order approximation. In particular, for time resolutions of less than 6 points per period, the numerical results obtained by the sixth-order approximation differ from the analytic results by less than 10%; however, this difference is greater than 24% for the second-order approximation. Thus, the second-order approximation can provide sufficiently accurate results when the temporal resolution is high; however, the higher-order finite-difference method for the time derivative is required to obtain accurate acoustic predictions if the temporal resolution is low, owing to the limited time step size. The calculation time of the prediction varies depending on the order of approximations to the time derivatives, and its comparison is listed in Table 1. When applying the sixth-order approximation, the calculation time increases by only 3%, as compared to that with the second-order approximation, owing to the increase in the amount of computation.

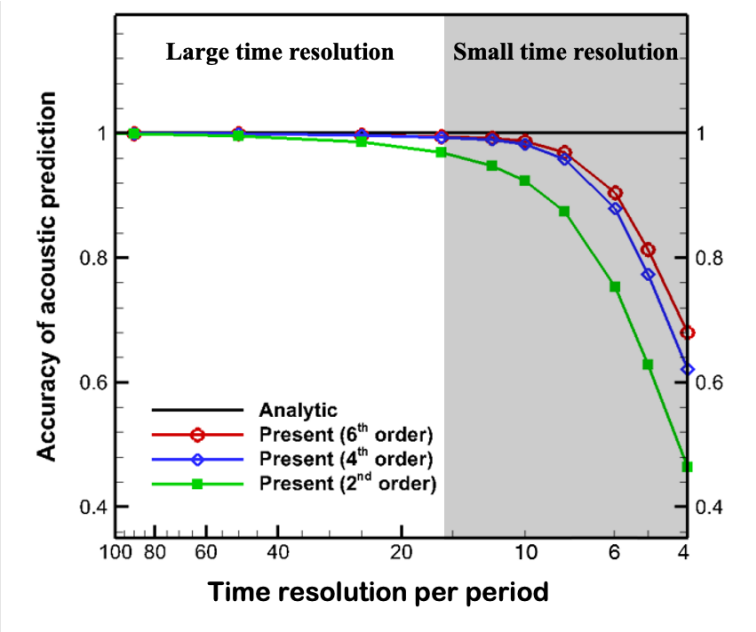

Fig. 8. Accuracy of far-field acoustic prediction obtained from second-, fourth-, and sixth-order finite-difference approximations of time derivatives depending on time resolutions per period

Table 1. Computing time depending on the order of approximations to the time derivatives

Order	Computing Time (s)	Difference (%)
2^{nd} order	3.36	-
4^{th} order	3.40	1.3%
6^{th} order	3.46	3.0%

4. Conclusion

This study aimed to improve the prediction accuracy of far-field radiated acoustic pressures with limited temporal resolutions using the formulae for high-order finite-difference approximations to the time derivative for the acoustic analogy. The time domain integral formulation of the acoustic analogy based on the FW–H equation was used for predicting the far-field acoustic pressure. The effects of the second-, fourth-, and sixth-order approximations of the time derivatives on the prediction accuracy were examined by comparing the numerical results with a known exact analytic solution. The comparison results showed that the acoustic analogy of

the fourth- and sixth-order approximations afforded 2–16% more accurate results than that of the second-order approximation in low time resolutions of 6–16 points per target period. For a time resolution of less than 6 points per period, the prediction results obtained by the sixth-order approximation indicated a difference of less than 10% from the analytic result; however, for the second-order approximation, this difference exceeded 24 %. Thus, the use of the higher-order finite-difference method for the time derivative in the acoustic analogy is an efficient approach to improve the prediction accuracy of the radiated acoustic pressure, particularly when the temporal resolution is not sufficiently high owing to the limited input conditions.

The findings of this study are expected to serve as a guide for predicting far-field acoustic propagation with the time-domain integral formulation of the FW-H equation using higher-order time derivatives. However, this study is limited in that it only calculates the prediction accuracies for sound propagation on the Kirchhoff surface with stationary monopole and dipole sources as input data, as it is challenging to obtain the exact solution for the moving monopole and dipole acoustic sources. In the future work, we aim to supplement the noise prediction accuracies for moving acoustic sources.

Declaration of competing for interest

The authors declare that they have no known competing financial interests or personal relationships that could have appeared to influence the work reported in this paper.

Acknowledgments

This study is supported by the National Research Foundation of Korea (NRF) grant funded by the Ministry of Science, ICT & Future Planning (NRF-2017-R1A5A1015311 and NRF-2021R1C1C1010198). This work is also supported by the Korea Agency for Infrastructure Technology Advancement (KAIA) grant funded by the Ministry of Land, Infrastructure and Transport (Grant RS-2022-00143965).

References

1. V. F. Kopiev, M. L. Shur, A. K. Travin, I. V. Belyaev, B. S. Zamtfort, and Y. V. Medvedev, Acoust. Phys. **63** (6), 723-730 (2017).
2. V. F. Kopiev, M. Y. Zaytsev, V. I. Vorontsov, S. A. Karabasov, and V. A. Anikin, Acoust. Phys. **63** (6), 686-698 (2017).
3. J. F. Williams and D. L. Hawkings, Philos. Trans. Royal Soc. A **264** 321–342 (1969).
4. K. S. Brentner and F. Farassat, Prog. Aerosp. Sci. **39** 83–120 (2003).
5. L. Yang, J. Huang, M. Yi, C. Zhang and Q. andiao, Acoust. Phys. **63** (6), 699-710 (2017).
6. M. J. Park and D. J. Lee, Appl. Acoust. **118** 66–75 (2017).
7. J. A. Visintainer, C. L. Burley, M. A. Marcolono and S. R. Liu, J. Am. Helicopter Soc. **38** 35-44 (1993).
8. P. F. Lorber, J. Am. Helicopter Soc. **36** 66–76(1991).
9. G. Faranosov, V. Goloviznin, S. Karabasov, V. Kondakov, V. Kopiev and M. Zaitsev, Comput. Fluids, **88** 165-179 (2013)
10. M. R. Visbal and D. V. Gaitonde, AIAA J. **37** 1231–1239 (1999).
11. T. Colonius and S. K. Lele, Prog. Aerosp. Sci. **40** 345–416 (2004).
12. I. Toulopoulos and J. A. Ekaterinaris, AIAA J. **44** 502–511 (2006).
13. M. Parsani, G. Ghorbaniasl and C. Lacor, J. Comput. Acoust. **19** 241–268 (2011).
14. P. R. Ziegenbein and B. K. Oh, *Proceedings of the AHS Specialists' Meeting on Aerodynamics and Aeroacoustics, (Arlington, TX, Feb. 25-27, 1987)*
15. C. Haigermoser, Exp Fluids **47**, 145–157 (2009).
16. V. Koschatzky, J. Westerweel, and B. J. Boersma. Phys. Fluids **23** 065112 (2011).
17. P. Moore, V. Lorenzoni, and F. Scarano, Exp Fluids **50** 877-885 (2011).
18. K. S. Brentner, C. L. Burley, and M. A. Marcolini, J. Am. Helicopter Soc. **39** 43-52 (1994).
19. D. A. Boxwell, F. H. Schmitz, W. R. Splettstoesser and K. J. Schultz, J. Am. Helicopter Soc. **32** 3-12 (1987).
20. G. A. Brès, K. S. Brentner, G. Perez and H. E. Jones, J. Sound Vib. **275** 719–738 (2004).
21. A. S. Morgans, S. A. Karabasov, A. P. Dowling and T. P. Hynes, AIAA J. **43** 1512–1524 (2005).

22. Z. Huang, L. S. Rousoulis, T. D. Troyer and G. Ghorbaniasl, Appl. Acoust. **140** 122–131 (2018).
23. M. J. Lighthill, Proc. Math. Phys. Eng. Sci. **211** 564–587 (1952).
24. M. J. Lighthill, Proc. Math. Phys. Eng. Sci. **222** 1–32 (1954).
25. N. Curle, Proc. Math. Phys. Eng. Sci. **231** 505–514 (1955).
26. M. V. Lowson, Proc. Math. Phys. Eng. Sci. **286** 559–572 (1965).
27. M. V. Lowson and J. B. Ollerhead, J. Sound Vib. **9** 197–222 (1969).
28. F. Farassat, NASA TP-3428 (1994).
29. F Farassat and K. S. Brentner, Theor. Comput. Fluid Dyn. **10** 155–170 (1998).
30. P. di Francescantonio, J. Sound Vib. **202** 491-509 (1997).
31. F. Farassat and M. Myers, J. Sound Vib. **123** 451–460 (1998).
32. A. S. Lyrintzis, J. Fluids Struct. **116** 665–676 (1994).
33. K. S. Brentner and F. Farassat, Prog. Aerosp. Sci. **39** 83–120 (2003).
34. L. Yang, J. Huang, M. Yi, C. Zhang and Q. andiao, Acoust. Phys. **63** (6), 699-710 (2017).
35. M. J. Park and D. J. Lee, Appl. Acoust. **118** 66–75 (2017).
46. K. S. Brentner and F. Farassat, AIAA J. **36** 1379–1386 (1998).
47. D. Lockard and J. Casper, *11th AIAA/CEAS Aeroacoustics Conference*, (Monterey, California, USA, May 23-25, 2005).
48. D. Casalino, J. Sound Vib. **261** 583–612 (2003).
49. M. Kessler and S. Wagner, Comput. Fluids, **33** 791-800 (2004).
40. K. S. Brentner, AIAA J. **35** 625–630 (1997).
41. H. Jeffreys and B. S. Jeffreys, *Methods of Mathematical Physics;* 3rd ed. (Cambridge University Press, 1972).
42. P. M. Morse and K. U. Ingard, *Theoretical acoustics* (Princeton University Press, New York, 1987).